# Parameterization of Orography-Induced Turbulence in a Mesobeta-Scale Model

P. BOUGEAULT AND P. LACARRÈRE

*Centre National de Recherche Météorologique, Toulouse, France*

(Manuscript received 21 April 1988, in final form 20 March 1989)

ABSTRACT

The possibility of extending existing techniques for turbulence parameterization in the planetary boundary layer to altitude, orography-induced turbulence events is examined. Starting from a well-tested scheme, we show that it is possible to generalize the specification method of the length scales, with no deterioration of the scheme performance in the boundary layer. The new scheme is implemented in a two-dimensional version of a limited-area, numerical model used for the simulation of mesobeta-scale atmospheric flows. Three well-known cases of orographically induced turbulence are studied. The comparison with observations and former studies shows a satisfactory behavior of the new scheme.

## 1. Introduction

The understanding and numerical simulation of weather events induced by orography are major challenges for mesobeta-scale meteorology (Orlanski 1975), as well as for the parameterization of kinetic energy dissipation in general circulation models. The numerical modeling of these flows offers great insight but present a number of specific difficulties, which have been pointed out by previous authors, for instance, Klemp and Lilly (1978) or Pielke (1984). Among these, the parameterization of the turbulent exchanges of heat and momentum becomes a more difficult problem in mountainous areas, since the dynamics of gravity waves generated by the terrain can increase the wind shear or decrease the static stability, thereby helping to generate turbulence, which in turn feeds back on the structure of the waves. Klemp and Lilly (1978) have pointed out the necessity of a good parameterization of the intense turbulence generated by wave breaking events to achieve correct numerical simulations of these processes. This has been confirmed in later work by Peltier and Clark (1979) and Durran and Klemp (1983).

The present paper is an attempt to take advantage of the recent development of parameterization schemes to forecast the turbulence kinetic energy (TKE), which originate from planetary boundary layer (PBL) studies, and are economical enough to be included into full three-dimensional mesoscale models. The primary motivation to undertake this study is to forecast the position and intensity of clear-air turbulence, which may have a number of important practical applications. It is also hoped that the feedback of the parameterization scheme on the model dynamics will improve the general quality of the simulation. This is, however, a more difficult task because some of the schemes previously used to parameterize turbulence are already able to describe much of the involved physics as soon as they include a significant dependence on the static stability.

In the authors' knowledge, only Beljaars et al. (1987), Richard et al. (1988, personal communication) and Buty (1988) have tried a similar approach based on a prognostic equation for the TKE. The study by Beljaars et al. is, however, restricted to the planetary boundary layer over a hill, whereas the present study, as well as the two other references, address disturbances that extend to the entire troposphere. Previous works on the modeling of orographic flows have used either empirical procedures or first-order closure schemes to specify the vertical and horizontal turbulence exchange coefficients. For instance, Klemp and Lilly (1978) used a turbulence adjustment procedure based on the idea that whenever the local Richardson number Ri drops below the critical value of 0.25, the mean fields of wind and potential temperature must be adjusted to reestablish dynamic stability, while conserving momentum, energy, mass, and hydrostatic balance. On the other hand, Peltier and Clark (1979) used the first-order closure scheme suggested by Lilly (1962), that reads:

$$K_m = (KDX)^2 \,\mathrm{def}(1 - \mathrm{Ri})^{1/2},$$

where $K_m$ is the mixing coefficient for momentum, def the magnitude of the deformation tensor, Ri the Rich-

*Corresponding author address:* Dr. Phillipe Bougeault, Centre National de Recherche Météorologique, 42, Avenue G. Coriolis—31057 Toulouse, Cedex, France.

ardson number, $DX$ the grid resolution and $K = 0.21$. For the eddy Prandtl number, they assumed $\mathrm{Pr} = K_m/K_h = 1$, where $K_h$ is the eddy diffusion coefficient for heat. Whenever $\mathrm{Ri} > 1$, they assumed $K_m = K_h = 0$. Durran and Klemp (1983) used a similar formulation, except for the eddy Prandtl number $K_m/K_h = \frac{1}{3}$. Thus, in their model, the mixing was not allowed if $\mathrm{Ri} > \frac{1}{3}$. Finally, Hoinka (1985) used a stability independent formulation

$$K_m = \alpha DX^3 \left|\frac{\partial \xi}{\partial X}\right|,$$

with $\alpha = 0.42$ and $\xi = (\partial w/\partial X) - (\partial u/\partial Z)$.

In the current practice of NWP models, stability-dependent schemes are widely used to specify the mixing coefficients. For instance, the French operational models use a version of the scheme by Louis et al. (1981) whereby the mixing coefficients take large values when the Richardson number is small or negative.

In contrast with these formulations, we have tried to embody the stability dependence in the TKE prognostic equation, and use the most simple formulation $K_m = K_h = C_K l_K (e)^{1/2}$, where $e$ is the TKE, $C_K$ a numerical constant, and $l_K$ a characteristic length scale defined in section 3b.

The paper proceeds as follows: the host model is briefly presented in section 2. The turbulence scheme is described in section 3, together with results of validation tests in the convective planetary boundary layer, and a comparison with former work on the turbulence generated by gravity waves. The model is then applied to three well-documented and well-known cases of flows over a mountain range, and the results are compared with observations.

## 2. The host model

The dynamical model used in this study is a two-dimensional version in $X$ and $Z$ of the French Weather Service Limited Area Model Péridot (Imbard et al. 1986; Bougeault 1986). Only 2D simulations are shown in this paper, but the generalization to the 3D frame is straightforward.

The model uses a terrain-following coordinate $\sigma = p/p_s$, where $p_s$ is the pressure at surface level. Prognostic equations are solved for $Z = \ln(p_s)$, the temperature $T$, and the horizontal wind velocity $U$. Defining $\dot{\sigma} = d\sigma/dt$, $\omega = dp/dt$, $Z_b$, $T_b$, $U_b$, the lateral boundary values for $Z$, $T$, $U$, and $\phi$ the geopotential, the governing equations read:

$$\frac{\partial Z}{\partial t} = -\frac{1}{p_s}\left\{\frac{\partial}{\partial X}(p_s U) + \frac{\partial}{\partial \sigma}(p_s \dot{\sigma})\right\} - K_D(Z - Z_b), \quad \text{(i)} \tag{1}$$

$$\frac{\partial T}{\partial t} = -U\frac{\partial T}{\partial X} - \dot{\sigma}\frac{\partial T}{\partial \sigma} + \frac{\omega}{p}\frac{R_a}{C_P}T + \left.\frac{\partial T}{\partial t}\right|_V + \left.\frac{\partial T}{\partial t}\right|_H - K_D(T - T_b), \quad \text{(ii) (iii) (i)} \tag{2}$$

$$\frac{\partial U}{\partial t} = -U\frac{\partial U}{\partial x} - \dot{\sigma}\frac{\partial U}{\partial \sigma} - \frac{\partial \phi}{\partial X} - R_a T\frac{\partial Z}{\partial X} + \left.\frac{\partial U}{\partial t}\right|_V + \left.\frac{\partial U}{\partial t}\right|_H K_D(U - U_b).. \quad \text{(ii) (iii) - (i)} \tag{3}$$

Here $R_a$ is the universal gas constant, and $C_P$ the specific heat at constant pressure for air.

In (1)–(3) we have included, beside the classical adiabatic terms, (i) boundary relaxation terms ($K_D$ being a constant which varies slowly from 0 inside the model domain to a large value at the boundary, see Appendix), (ii) vertical diffusion terms, and (iii) horizontal diffusion terms. The formulation of these terms will be discussed below. The numerical discretization uses standard second-order accurate formulations (see Appendix).

When using the model on steep slopes, care must be taken that the horizontal diffusion terms do not induce spurious circulations. For the sake of simplicity, it is a common practice in large-scale atmospheric models to use constant diffusion coefficients, and to compute the gradients along coordinate surfaces. As shown by several authors (e.g., Alpert and Neumann 1984), this procedure is producing undesirable artifacts in mesobeta-scale models. Thus, we use the chain rule to evaluate the $X$ derivatives along true $p$ surfaces and write the horizontal diffusion operator as

$$\left.\frac{\partial \alpha}{\partial t}\right|_H = \left(\left.\frac{\partial}{\partial X}\right|_\sigma + \left.\frac{\partial \sigma}{\partial X}\right|_p \frac{\partial}{\partial \sigma}\right) K_H \left(\left.\frac{\partial}{\partial X}\right|_\sigma + \left.\frac{\partial \sigma}{\partial X}\right|_p \frac{\partial}{\partial \sigma}\right)\alpha, \tag{4}$$

for $\alpha = U$ and $T$. The horizontal diffusion coefficient $K_H$ is related to the grid size $\Delta X$ of the model by $K_H = U_2 \Delta X$, $U_2$ being a velocity scale set to 4 m s$^{-1}$ in the present experiments. The above formulation has been tested extensively by comparison with solutions without diffusion and is performing satisfactorily. In particular, we checked that if the model atmosphere is initially at rest, no circulation is generated by the diffusion terms.

The vertical diffusion terms are given the standard expressions

$$\left.\frac{\partial T}{\partial t}\right|_V = -\frac{1}{\rho}\frac{T}{\theta}\frac{\partial}{\partial Z}\rho\overline{w'\theta'}, \quad \left.\frac{\partial U}{\partial t}\right|_V = -\frac{1}{\rho}\frac{\partial}{\partial Z}\rho\overline{w'u'}, \tag{5}$$

$\theta$ being the potential temperature and $\rho$ the air density.

For all levels but the surface, the vertical turbulent fluxes $\overline{w'\alpha'}$ are computed by the turbulence scheme (see section 3), using vertical diffusion coefficients, which depend on the TKE. At the surface level, the vertical turbulent fluxes are computed through bulk transfer formulae:

$$\overline{w'\alpha'_s} = -C_\alpha \| V_N \| (\alpha_N - \alpha_S), \qquad (6)$$

where $V_N$, $\alpha_N$ stand for the model-predicted values at the lowest level and $\alpha_s$ is the surface value (assumed constant in time for the present study). The transfer coefficients $C_\alpha$ follow Louis et al. (1981), reading

$$C_\alpha = \{k/\ln(Z_N/Z_0)\}^2 f_\alpha(\mathrm{Ri}), \qquad (7)$$

where $k$ is the von Kármán constant ($k = 0.4$), $Z_N$ is the height of the lowest model level above the surface, and $f_\alpha(\mathrm{Ri})$ are stability-dependent functions. In the experiments shown in sections 4, 5 and 6, the roughness height $Z_0$ is given the value 0.1 m and $Z_N$ is taking values ranging from 125 to 250 m.

Finally, it is necessary to prevent the reflection of upward propagating internal gravity waves at the top of the model. This is achieved by the use of an absorbing layer, following Klemp and Lilly (1978). The model dynamics has been tested extensively (Bougeault 1987, 1988) following the suggestions of previous authors, on linear and nonlinear cases. As an example, Fig. 1 shows the linear response of the model when an isothermal ($T = 273$ K) atmosphere with uniform mean wind ($U = 20$ m s$^{-1}$) passes over a bell-shaped mountain with a 50 m height and a 25 km half-width. The results have been amplified by a factor of 10 for the purpose of visualization, and the linear analytic solution is shown for comparison. The version of the model used for this test has 160 grid points on the horizontal, with $\Delta X = 5$ km, and 40 grid points on the vertical, with $\Delta Z = 500$ m. The absorbing layer is defined between 15 and 20 km height. The solution shown in Fig. 1 is a 24 hour simulation, which corresponds to the nondimensional $tU/d = 34$ with Klemp and Lilly's (1978) notations. The vertical momentum flux at the same time is compared with the theoretical value in Fig. 1b.

Other tests have included simulations of the Boulder windstorm of 11 January 1972, made with a version of the model designed to be as similar as possible with previously published studies: The subgrid-scale mixing was parameterized through the stability dependant scheme of Louis et al. (1981), and a free-slip condition was applied at the lower boundary. These tests compared well with published results (Klemp and Lilly 1978; Peltier and Clark 1979; Durran and Klemp 1983; Hoinka 1985; Richard et al. 1985). Finally, an investigation of the model results sensitivity with several modifications of the upstream profiles on this same case gave results in complete agreement with those of Durran (1986) and Durran and Klemp (1987).

## 3. The turbulence scheme

### *a. TKE prognostic equation*

The scheme used in the present study has evolved from the work of Therry and Lacarrère (1983, TL83 hereafter). This so-called "one-and-a-half order" closure scheme is based on a prognostic equation for the turbulence kinetic energy $e$ [$e = \frac{1}{2}(u'^2 + v'^2 + w'^2)$]:

$$\frac{\partial e}{\partial t} = -\frac{1}{\rho}\frac{\partial}{\partial Z}\rho\overline{w'e'} - \overline{u'w'}\frac{\partial U}{\partial Z} - \overline{v'w'}\frac{\partial V}{\partial Z} + \beta\overline{w'\theta'} - \epsilon, \qquad (8)$$

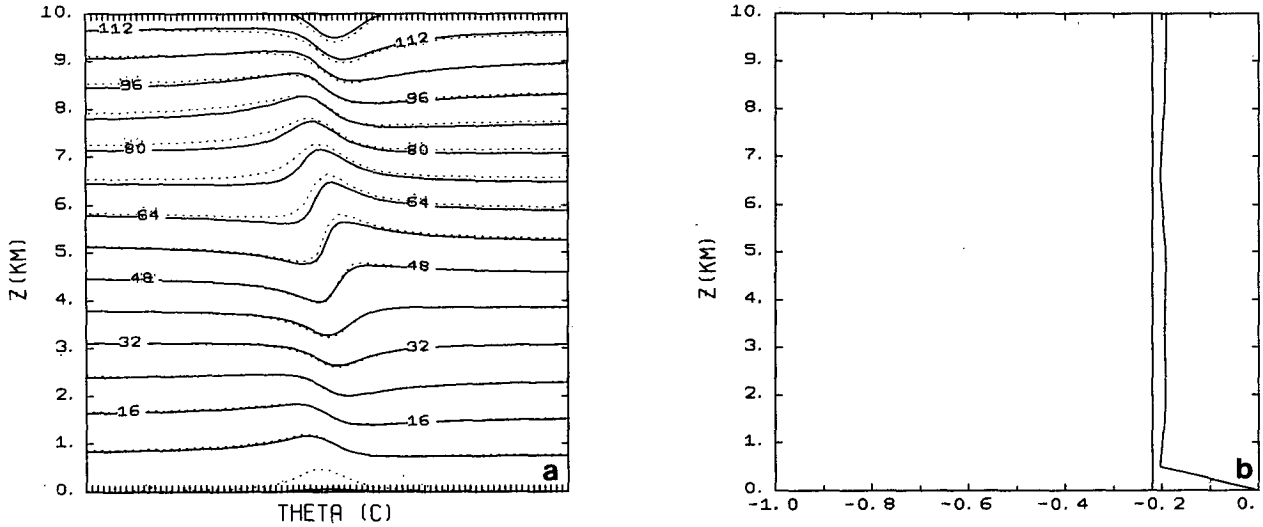


FIG. 1. A comparison of the model steady-state result with the analytical solution for the flow past a bell-shaped mountain. (a) Cross section of potential temperature; solid line—model result; dashed line—analytical solution. The distance between two ticks on the horizontal axis is 5 km. (b) The profile of the momentum flux (Pa) computed by the model, as compared to the theoretical value.

where $\beta$ is the buoyancy coefficient ($\beta = g/T$), and $\epsilon$ the dissipation of TKE by molecular processes.

The second-order moments appearing in Eq. (8) are parameterized according to an eddy coefficient approximation:

$$\overline{w'u'} = -K_m \frac{\partial U}{\partial Z},$$

$$\overline{w'v'} = -K_m \frac{\partial V}{\partial Z},$$

$$\overline{w'e'} = -K_e \frac{\partial e}{\partial Z},$$

$$\overline{w'\theta'} = \begin{cases} -K_h\left(\dfrac{\partial \theta}{\partial Z} - \gamma_{cg}\right), & \text{in the convective PBL} \\ -K_h \dfrac{\partial \theta}{\partial Z}, & \text{elsewhere.} \end{cases} \tag{9}$$

The vertical diffusion coefficients are related to the TKE through:

$$K_m = C_K l_K e^{1/2}, \quad K_h = \alpha_T K_m, \quad K_e = \alpha_e K_m,$$

where $C_K$ is a numerical coefficient, and $l_K$ a characteristic length for the eddies. The inverse turbulent Prandtl numbers $\alpha_T$ and $\alpha_e$ are given the values $\alpha_T = \alpha_e = 1$ (note that this value was 1.3 in TL83).

The constant $\gamma_{cg}$ in (9c) is the so-called "countergradient" correction (Deardorff 1972), which applies only in the convective PBL, and allows for slightly stable stratification persisting with upward heat flux. We have retained this aspect of the original scheme, although it probably has little significance for the present study.

Finally, the TKE dissipation is estimated by the classical relation

$$\epsilon = C_\epsilon e^{3/2}/l_\epsilon, \tag{10}$$

where $C_\epsilon$ is an O(1) numerical coefficient, and $l_\epsilon$ a characteristic length of the energy-containing eddies.

### b. *Specification of the length scales $C_K l_K$ and $l_\epsilon/C_\epsilon$*

In the original version of the scheme (Therry and Lacarrère 1983) the characteristic length scales have been adjusted to fit a large number of experimental data on turbulence in the convective PBL. As a consequence, they were parameterized by rather involved expressions, which unfortunately have no counterparts outside the PBL. When trying to use this scheme for orography-induced turbulence, we need to find a specification that is as simple as possible and more general, and that would supply similar values as the former version in the PBL. This may be achieved by generalizing the basic scaling factors of TL83 formulations, which are the distance to the surface and the distance to the inversion at the top of the PBL. Such a scheme has been proposed by Bougeault and André (1986) in the context of a third-order turbulence model, and may be adapted here.

We postulate that for each level in the atmosphere $l_\epsilon$ and $l_K$ can be related to the distance that a parcel originating from this level, and having an initial kinetic energy equal to the mean TKE of the layer, can travel upward and downward before being stopped by buoyancy effects. More precisely, if we define $l_{up}$ and $l_{down}$ by

$$\int_Z^{Z+l_{up}} \beta(\theta(Z) - \theta(Z'))dZ' = e(Z), \tag{11a}$$

$$\int_{Z-l_{down}}^{Z} \beta(\theta(Z') - \theta(Z))dZ' = e(Z), \tag{11b}$$

$l_K$ and $l_\epsilon$ must be related to some average value between $l_{up}$ and $l_{down}$. The main advantage of the method is to allow for remote effects of stable zones on the definition of the turbulence length scales. For instance, using Eq. (11), the vertical depth of an unstable layer capped by a strong inversion is automatically selected as the length scale for turbulence. Moreover, close to the surface, the lower bound for the integral in (11b) is clearly 0, and the height above the surface $Z$ is introduced simply as the relevant length scale. Finally, in a layer of constant stratification $\partial\theta/\partial Z$, Eq. (11) provides an expression which is readily proportional to the buoyancy length scale

$$l_B = e^{1/2}\left(\beta \frac{\partial \bar{\theta}}{\partial Z}\right)^{-1/2}.$$

Careful consideration must be given to the way of averaging $l_{up}$ and $l_{down}$, since in all regions where $l_{up} \gg l_{down}$ or inversely, the order of magnitude of the average will depend on the type of averaging operator. We feel that for the mixing length scale $l_K$, it is convenient to choose an averaging operator that has a bias towards the smaller of $l_{up}$ and $l_{down}$, since it is well established that the diffusion coefficient near a wall varies with the distance to the wall, and we assume that the region of increased static stability that limits on the vertical the extension of turbulence acts like a kind of wall. We therefore choose $l_K = \min(l_{up}, l_{down})$ (a quite special average).

On the other hand, such a behavior is not established for the dissipative length $l_\epsilon$. On the contrary, it is observed that in convective boundary layers, the depth of the layer influences the size of the energy-containing eddies down to a very low height above the surface. Thus, we choose the formulation $l_\epsilon = (l_{up} l_{down})^{1/2}$. Note that these two averaging methods are different from the one used by Bougeault and André (1986). Finally, the inspection of a variety of experimentally determined values of dissipation rate (for instance, Fig. 5 of TL83) allows for the determination of $1/C_\epsilon$ as 1.4. Similarly, the value of $C_K$ is set to 0.4.

*c. Test of the new scheme on a convective PBL*

Since the definition of $C_K L_K$ and $l_\epsilon / C_\epsilon$ and the values of the turbulent Prandtl number $\alpha_T$ and $\alpha_e$ are changed from the original scheme, it is necessary to repeat at least some of the qualification tests of the model. This is done in repeating the Voves 2 and 3 July 1977 1D-simulation shown in TL83. This field experiment allowed for observations of the classical diurnal and nocturnal evolution of the PBL during an undisturbed, anticyclonic period with a weak mean wind divergence (2 July), followed by a period of moderate cold advection (3 July). It provided an ample dataset to validate 1D numerical models of the PBL. For a more complete discussion of this situation and of the numerical simulations, the reader is referred to André and Lacarrère (1980). A comparison between the modeled and observed evolution of the potential temperature profile during the 30-h simulated period is shown in Fig. 2. The model clearly does a good job in reproducing this evolution. These results are very close to those produced by the former version of the scheme. It is of interest that the model is able to reproduce correctly the evolution of the temperature

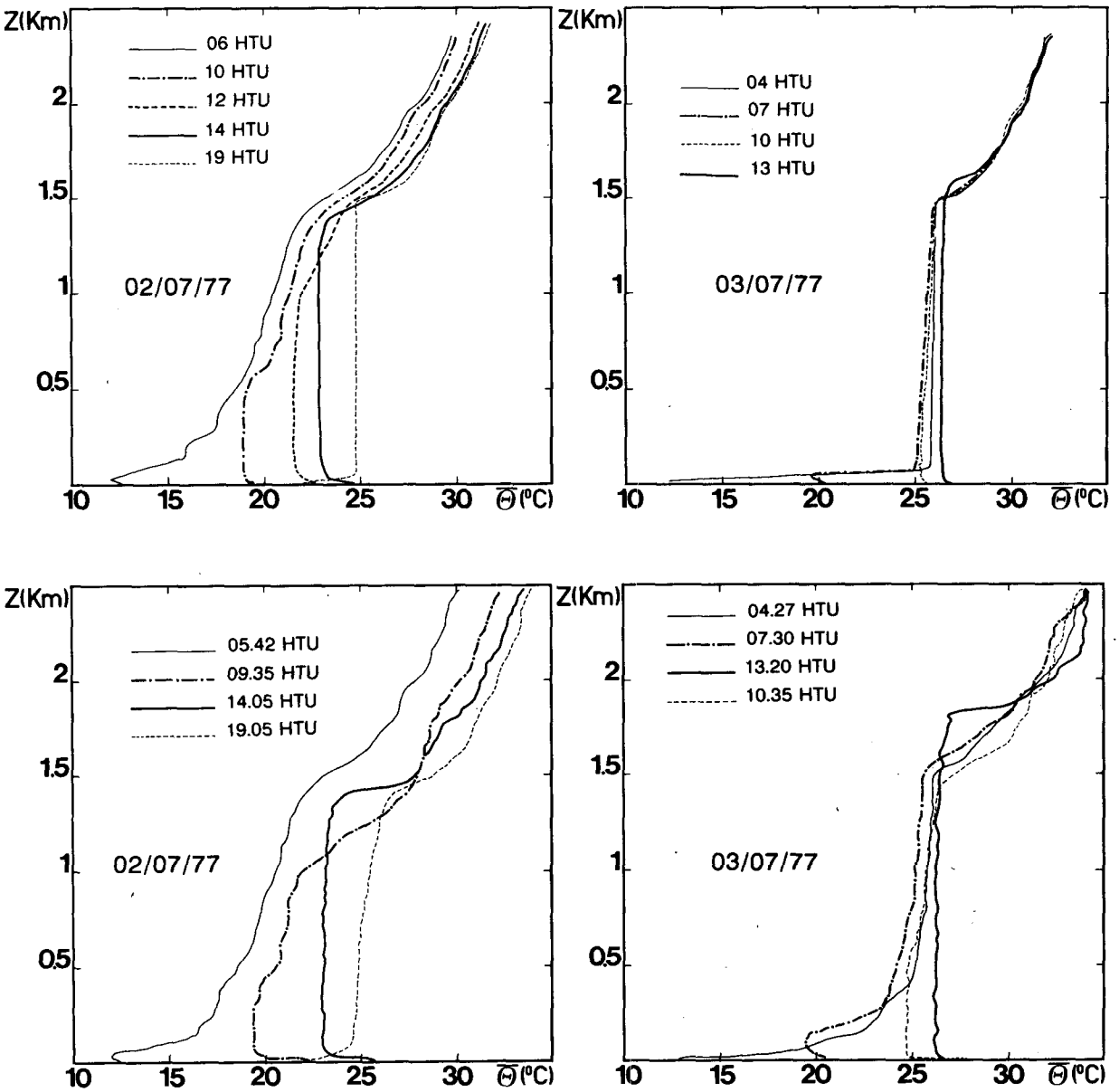


FIG. 2. A reassessment of TL83 PBL model based on Eq. (8), with the new specification of the length scales. Simulated (upper panel) and observed (lower panel) potential temperature profiles on 2 and 3 July, 1977 on Voves (France). (HTU means Universal Time Hour).

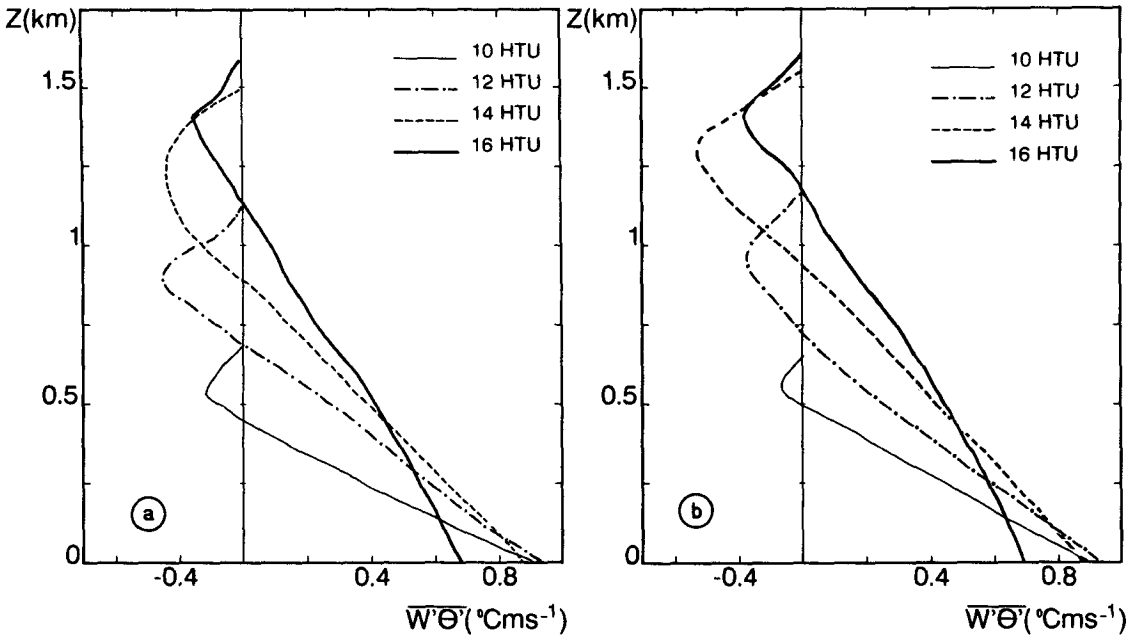


FIG. 3a. The vertical profiles of the turbulent heat flux stimulated by the TL83 model with the old (Panel a) and new (Panel b) specification of the length scales.

profile both on 2 July, when conditions of convective heating prevailed, and on 3 July, where the temperature hardly changed because of cooling by advection. The turbulence fluxes of heat predicted for 2 July with the old and new versions of the scheme are shown in Fig. 3a. They exhibit the familiar, linear decrease with $Z$, and negative values in the entrainment zone at the top of the mixed layer. We note the similarity of these two

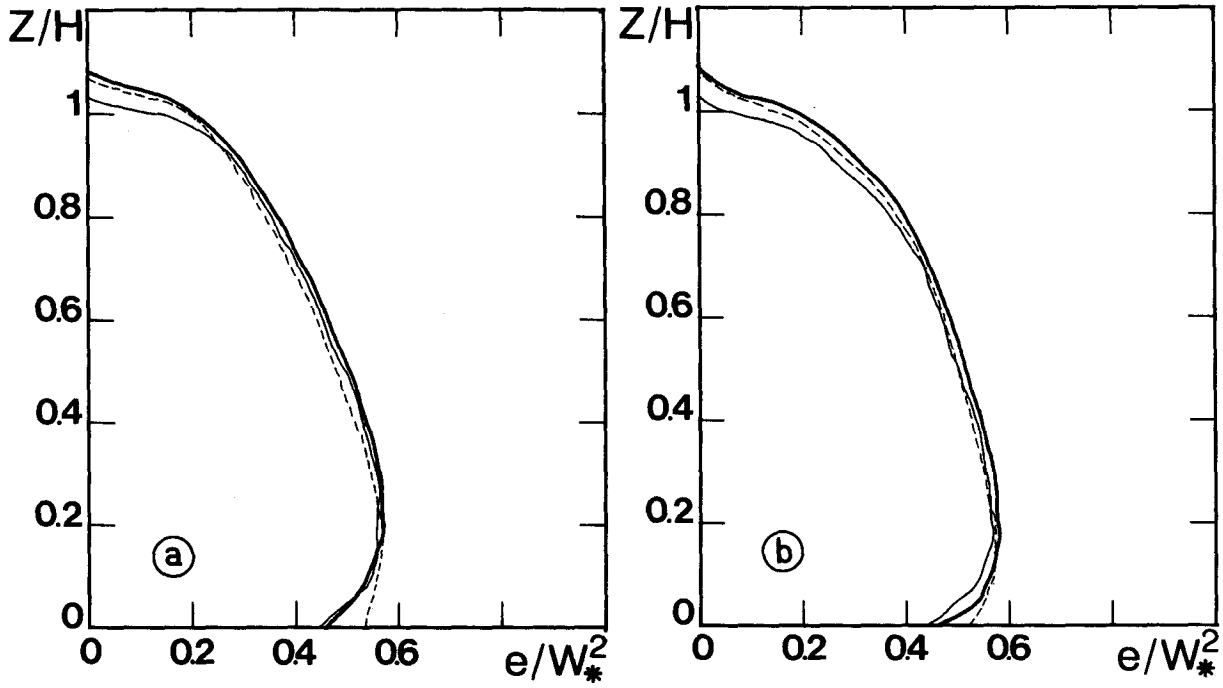


FIG. 3b. The vertical profile of normalized turbulence kinetic energy simulated by the TL83 model with the old (Panel a) and new (Panel b) specification of the length scales. The three profiles correspond to 2 July 1977 at 1200 UTC (dashed line), 1400 UTC (thick solid line) and 1600 UTC (thin solid line).

results. Next, the turbulence kinetic energy simulated at three different times, again with the old and new schemes, is shown in Fig. 3b. The result is normalized by the usual convective velocity scale $w_* = (\beta \overline{w'\theta'_s} H)^{1/3}$, $H$ being the height of the mixed layer. This is a severe way to test the performance of a model. We note that the normalized result is independant of time, as expected from the theory. Again, it can be seen that the changes made in the definition of the mixing and dissipation length scales have not modified the energetics of the PBL. Finally, the old and new formulations of the dissipative length scale $l_\epsilon/C_\epsilon$ are favorably compared to a variety of observations in Fig. 4. As a conclusion of this section, we can state that a more general formulation of the length scales has been defined, which does not deteriorate the results of the scheme for cases already simulated, and which allows for treating cases outside the PBL.

### d. Comparison with other theoretical formulations

It is of interest to see how our scheme compares with the formulation used in previous studies of turbulence generated by gravity waves. A summary of relevant work is given by Weinstock (1987, W87 hereafter). Both W87 and Fua et al. (1982) have used "one-and-a-half" order schemes, very comparable to our formulation. Therefore, only the closure hypothesis need to be compared. We will limit ourselves to the formulation of W87 hereafter.

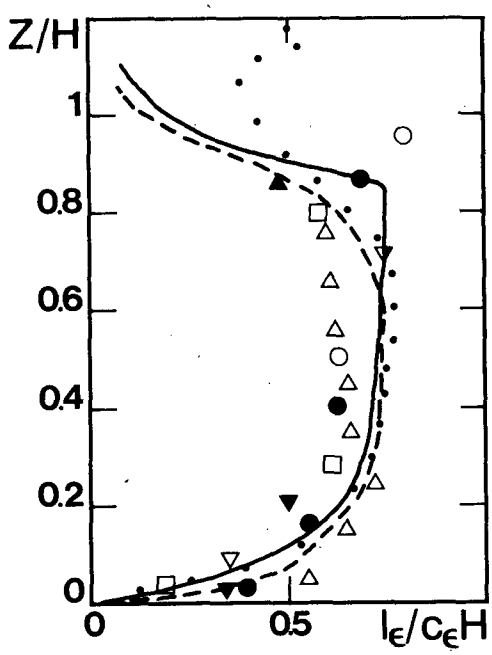


FIG. 4. An assessment of the specification of the dissipative length scale $l_\epsilon/C_\epsilon$. Dashed line—new formulation; solid line—old formulation. Experimental determinations: Lenschow et al. (1980) (● $H$ = 1010 m; □ $H$ = 1200 m; ▼ $H$ = 1430 m; ○ $H$ = 1200 m; Willis and Deardorff (1974): △ Deardorff (1974) (· · ·).

In conditions of unstable density stratification, W87 uses $\epsilon = 0.24 k_0 e^{3/2}$, and $K_m = (2/3e)^{1/2}(3k_0)^{-1} \approx 0.27 e^{1/2} k_0^{-1}$. Here, $k_0$ is the wave number of energy-containing eddies, and W87 postulates that $k_0$ can be related simply to the depth $L_0$ of the unstable region by $k_0 = 2\pi/L_0$. In our formulation, assuming an unstable region of depth $L_0$, limited on the vertical by two stable areas, (11) will supply $l_{up} = l_{down} \approx L_0/2$ for the central point of the unstable zone. Thus, we will compute $l_K = l_\epsilon = 2\pi/2k_0$, therefore $\epsilon = e^{3/2}/(1.4 \times 2\pi/2k_0) \approx 0.23 k_0 e^{3/2}$ and $K_m = 0.4(2\pi/2k_0)e^{1/2} \approx 1.25 e^{1/2}/k_0$. For given values of $e$ and $k_0$, our scheme will therefore supply the same estimate of $\epsilon$ as W87, and a value five times larger for $K_m$. We probably should not worry too much about the discrepancy on $K_m$, since as noted by the author himself, his computation involves a large degree of uncertainty, and the results are merely qualitative. We note, however, that a value of $K_m$ five times smaller in the PBL test reported in section 3c would not supply a correct evolution of the PBL structure. It may be hoped, however, that the similarity between our formulation and W87 will allow for qualitatively similar behavior of the two models.

Turning now to conditions of stable density stratification, the comparison with W87 is made more difficult because of the collapse condition he advocates. This may be summarized in the following way: for given Brunt–Väisälä frequency $N$ and $k_0$ values, the turbulence kinetic energy should be set to zero whenever $N/(2/3e)^{1/2} > k_0$, to simulate the effect of rapid energy dispersion by gravity waves. Such a condition cannot be implemented in our model, since these quantities are strongly related in regions of stable stratification. In fact, solving (11) for conditions of vertically uniform $N$ and $e$ supplies the condition: $l_{up} = l_{down} = (2e)^{1/2}/N$. Therefore, we will compute $L_0/2 = 2\pi/2k_0 = (2e)^{1/2}/N$, which gives: $N/(2/3e)^{1/2} \approx 0.55 k_0$, and the collapse condition will never be satisfied. The qualitative behavior of the two models may not be very different, however, because W87 uses a constant determination of $k_0$ in time, which is equivalent to stating that the turbulence length scale is determined by a memory of the most unstable conditions encountered during the gravity wave period. On the contrary, in our scheme, $l_{up}$ and $l_{down}$ are updated at every time step during the model integration, resulting in a strong damping of turbulence as soon as stable conditions are encountered. This may represent the very mechanism which is simulated by W87 collapse condition. Finally, it is of interest to compare our estimate for the ratio $K_m/\epsilon$ under stable conditions to theoretical predictions. Lilly et al. (1974) have proposed $K_m/\epsilon = (3N^2)^{-1}$, and Weinstock (1978) has demonstrated a more accurate formulation $K_m/\epsilon = 0.8/N^2$. Using again $l_{up} = l_{down} = (2e)^{1/2}/N$, we find $K_m = 0.4\sqrt{2}e/N$ and $\epsilon = eN/(1.4\sqrt{2})$. Thus $K_m/\epsilon = 1.4 \times 0.8/N^2$. The predictions therefore agree within a 1.4 factor, which can be thought reasonable, given the limits of the theoretical

computation. We conclude that our simple formulation is in reasonable agreement with former theoretical work.

*e. Inclusion of the turbulence scheme into the meso-beta-scale model*

When including the turbulence scheme in the model to represent horizontally nonhomogeneous cases, it is necessary to include in Eq. (8) two types of additional terms: advection and production by horizontal shear. Based on the following considerations, we assume that the production by horizontal shear can be neglected as a first approximation. The expanded form of the shear production term of TKE, for a two-dimensional model, reads:

$$p_d = \underbrace{-\overline{u'w'}\frac{\partial U}{\partial Z}}_{[1]} \underbrace{-\overline{v'w'}\frac{\partial V}{\partial Z}}_{[2]} \underbrace{-\overline{u'^2}\frac{\partial U}{\partial X}}_{[3]} - \underbrace{\overline{u'w'}\frac{\partial W}{\partial X}}_{[4]} \underbrace{-\overline{w'^2}\frac{\partial W}{\partial Z}}_{[5]}. \quad (12)$$

Assuming a nearly isotropic turbulence, $\overline{u'^2} \sim \overline{w'^2}$, terms 3 and 5 cancel each other because $\partial U/\partial X + \partial W/\partial Z = 0$. An *extreme* value of $\partial W/\partial X$ can be estimated, by inspection of observational and numerical results on the Boulder windstorm (see section 5), to $10^{-3}$ s$^{-1}$ (a gradient of 20 m s$^{-1}$ per 20 km). On the other hand, a reasonable value of $\partial U/\partial Z$ in the region of intense turbulence would be $10^{-2}$ s$^{-1}$ (a gradient of 10 m s$^{-1}$/km). Therefore, there is at least an order of magnitude difference between the vertical and horizontal shear production terms. Of course, these estimations are locally wrong in those areas when $\partial U/\partial Z$ takes small values, but this may not be important since the TKE is usually small at these places. Numerical tests including all the terms of Eq. (12) are required to verify our assumption. Also, it should be noted that this analysis is highly scale-dependent. For models of mesogamma scale, which resolve a larger part of the spectrum of vertical motions, it would be incorrect to assume that the production by horizontal shear can be neglected. The advection of TKE, on the other hand, is by no means negligible, and is included in Eq. (8). The full form of the TKE equation implemented in the mesoscale model reads therefore:

$$\frac{\partial e}{\partial t} = -U\frac{\partial e}{\partial X} - \dot{\sigma}\frac{\partial e}{\partial \sigma} - \frac{1}{\rho}\frac{\partial}{\partial Z}\rho\overline{w'e'} - \overline{u'w'}\frac{\partial U}{\partial Z} - \overline{v'w'}\frac{\partial V}{\partial Z} + \beta\overline{w'\theta'} - \epsilon. \quad (13)$$

Note that there is no advection along $V$ since the model is 2D; however, $V$ is not zero, and the production of energy by the shear of the $V$ component is taken into account.

## 4. Simulation of the bora observed on 6 March 1982

The bora is a severe northeasterly downslope wind off the mountains along the Adriatic coast of Yugoslavia. Several events have been documented by aircraft during the ALPEX experiment field phase (Spring 1982). Analyses of these data, including TKE vertical cross sections, have recently been published by Smith (1987) and Pettré (1988). We have selected the case of 6 March 1982 as particularly appropriate to test our model. An upstream sounding for this case, (courtesy of P. Pettré) is shown in Fig. 5. Northeasterly flow in the lower layers rotates southeasterly above the inversion near 3 km altitude. To simulate this case in the 2D model, we assume that the mountain range can be considered roughly two-dimensional, oriented northwest to southeast, i.e., perpendicular to the low-level wind. The horizontal and vertical grid size are chosen as $\Delta X = 5$ km and $\Delta Z = 250$ m. One may question if this horizontal resolution is adequate to resolve the steep lee-slope. The present work, however, is primarily directed to the qualification of a mesobeta scale, hydrostatic model. It would not be reasonable to increase further the resolution of the model without additional damping of the shortest waves. An alternative solution would be to smooth the mountain profile. In view of the results presented below, smoothing does not seem necessary in this case. The model has 43 grid points on the horizontal and 30 on the vertical. The absorbing layer is defined between 5 and 7.5 km altitude. The

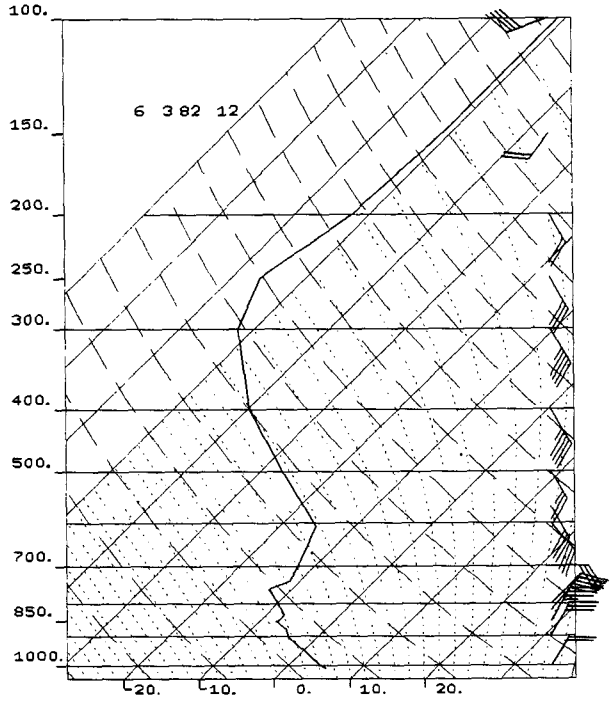


FIG. 5. Sounding at Zagreb, Yugoslavia, 1200 UTC 6 March 1982 used as initial condition in the model.

topography is obtained from the downward looking radar of the aircraft. The model is initialized with uniform data corresponding to the sounding in Fig. 5, and the same data are used as boundary relaxation values during the simulation. The model reaches a stationary state after roughly 4 h of simulated time. The results after 6 h are shown on Fig. 6. For comparison, the vertical cross sections of $U$, $W$, and $\theta$ produced by Pettré (1988) are shown in Fig. 7, together with the cross section of vertical velocity variance by Smith (1987) on Fig. 8. The simulation is in agreement with these observations below the linear critical level ($U = 0$) occurring at $Z = 4$ km. The wind gradually accelerates when approaching the crest and reaches a maximum value larger than 25 m s$^{-1}$ on the downstream slope, but it recovers quickly through a hydraulic jump. The vertical velocities reach $-1.5$ m s$^{-1}$ on the downslope side. A return flow is observed right over the crest at $Z = 3$ km. Note that these results are in qualitative agreement with those of previous numerical simulations. Hoinka (1985) has simulated the bora of 7 March 1982 and Klemp and Durran (1987)

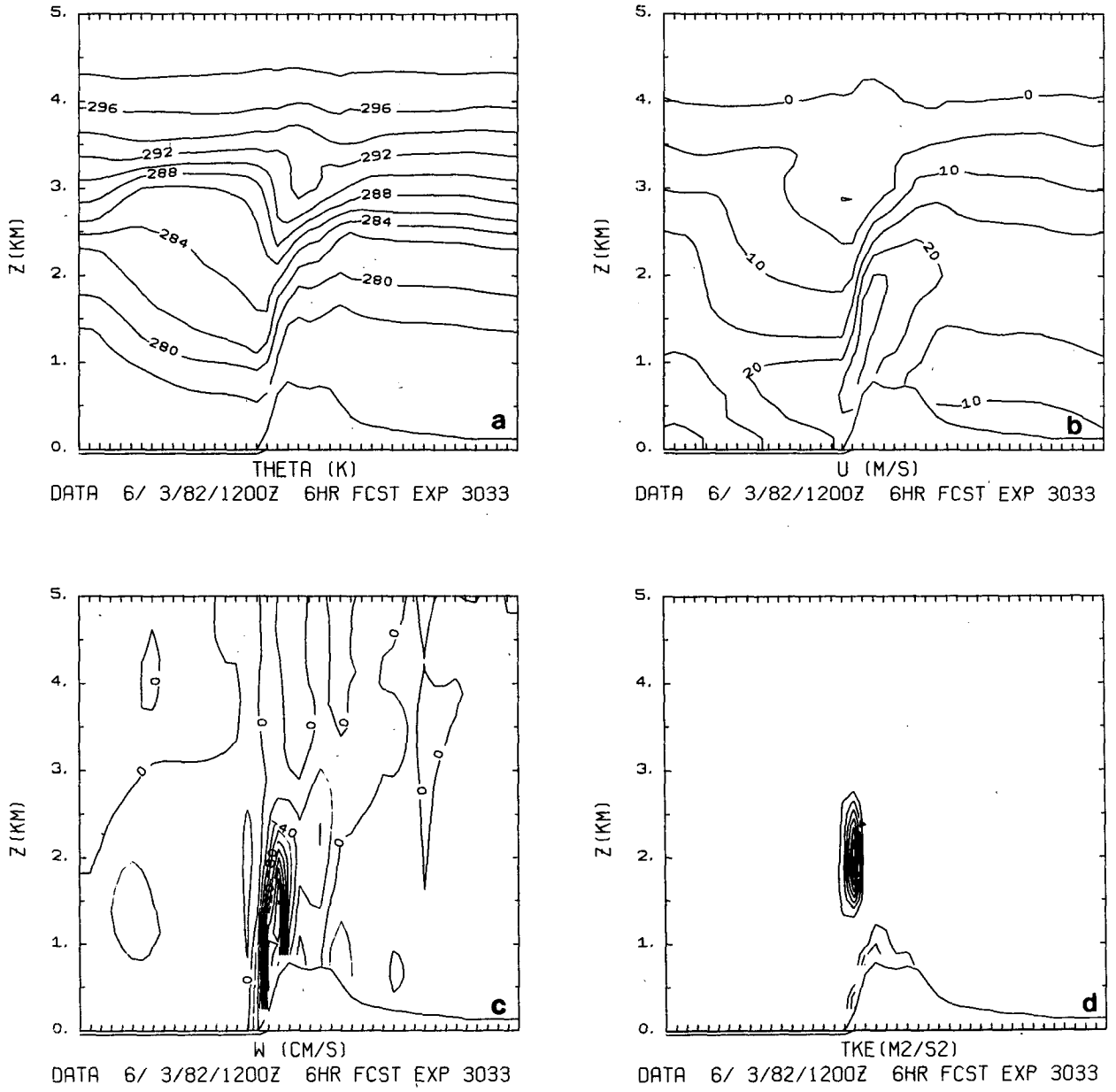


FIG. 6. Results of the simulation of 6 March 1982, after the steady state is reached. (a) Potential temperature. (b) Horizontal wind. (c) Vertical velocity. (d) Turbulence kinetic energy [the isoline interval is 2 (m s$^{-1}$)$^2$], starting at 2 (m s$^{-1}$)$^2$. Note that the mean flow is from the right to the left of the picture. Ticks are every 5 km on the horizontal axis.

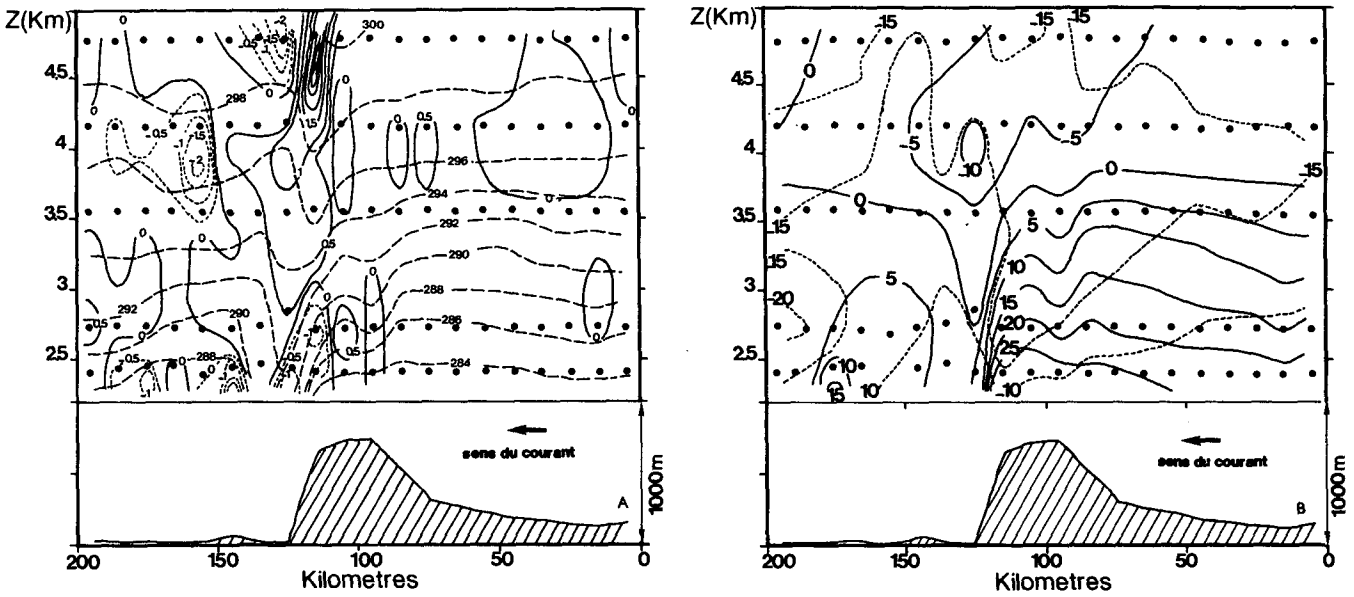


FIG. 7. From Pettré (1988); cross section of mean flow parameters obtained from an analysis of aircraft data on 6 March 1982. (a) Potential temperature (dashed) and vertical velocity (solid). (b) Horizontal wind perpendicular to the range (solid) and parallel to the range (dashed). The dots indicate the points where the basic data have been obtained.

have simulated the bora of 15 April 1982. There is a close similarity between the upstream soundings of all three cases, which show low-level northeasterly winds surmounted by an inversion of temperature, containing a linear critical level induced by the wind rotation. We may therefore consider these three cases as slight variations of the same mechanism. The turbulence develops in the region of low static stability corresponding

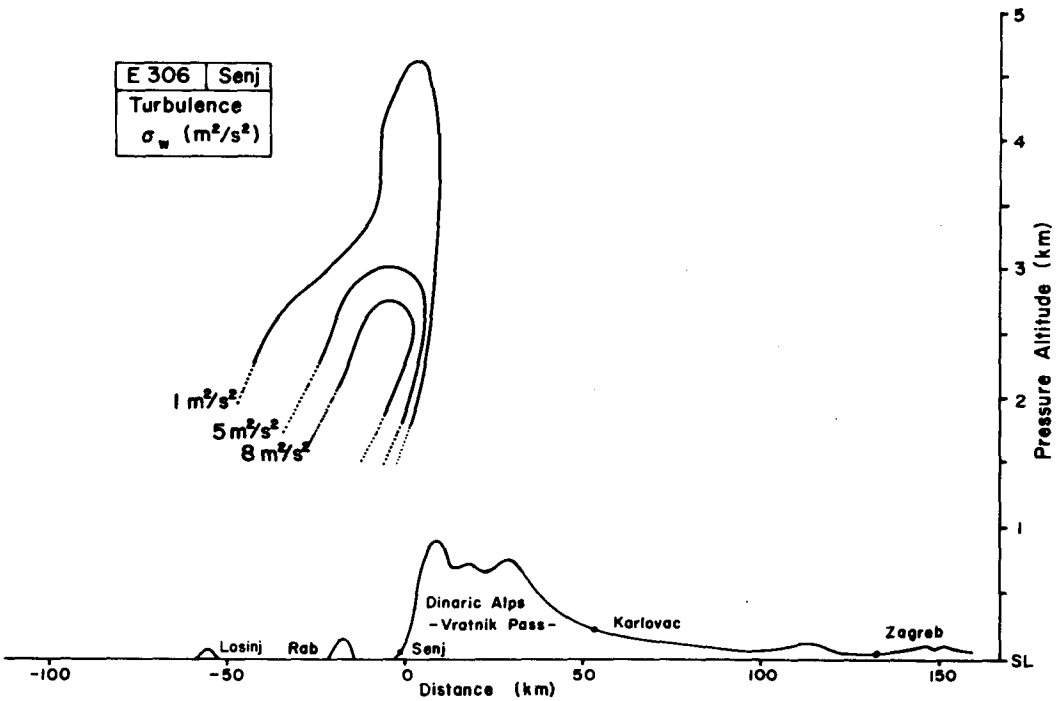


FIG. 8. From Smith (1987); turbulence cross section for 6 March 1982. Vertical velocity variance over 10 sec. (1300 m) of the flight track is shown with no trend removal. Leeside turbulent region has a width of 40 km and a depth of 2 to 3 km (Smith's comment).

to the ascending branch between $Z = 1$ km and $Z = 3$ km, with intensity reaching more than 10 $(\text{m s}^{-1})^2$. This is in remarkable agreement with Smith (1987) observations if we assume that the vertical velocity variance is a good estimate of the total TKE. There is also an appreciable amount of turbulence near the surface, but no data are available to estimate if its intensity is realistic.

Above the linear critical level, the model results are at variance with the observations. The wave energy is not propagating beyond $Z = 4$ km, as might be expected from the theory. In the observations, strong updrafts and downdrafts are seen to occur near $Z = 4.5$ km. We suspect that the three-dimensional character of the real topography may explain this discrepancy as well as the fact that the zero wind line dips much lower in the observations than in the simulation. In fact, when looking at a topography map of the area, it is clear that the gravity wave field cannot be 2D; as noted by a reviewer, this may also be inferred from the fact that the $V$-component cross section shown in Fig. 7b exhibits significant structures. Thus, a significant amount of wave components are able to propagate upward, and may explain the observations. When running the simulation with a uniform upstream wind of 20 m $\text{s}^{-1}$ above the inversion, we were able to obtain a qualitatively correct description of the vertical velocity at $Z = 4.5$ km (not shown).

## 5. Simulation of a stationary mountain wave observed on 17 February 1970

The second test case is provided by observations of Lilly and Kennedy (1973, LK73 hereafter) over the Rocky Mountains. This well-known case has been simulated by Klemp and Lilly (1978) and Hoinka (1985). An upstream sounding for this case can be found in the former paper. Strong winds are blowing from the west throughout the troposphere, and the tropopause is very high (80 hPa). To simulate this case, we retain $\Delta X = 5$ km, but use 50 levels with $\Delta Z = 600$ m. The absorbing layer is defined between 25 and 30 km. The topography is approximated by a bell-shaped mountain with height 2000 m, and half-width $a = 10$ km, following previous modeling studies. The results of the model after 6 h of simulated time are shown on Fig. 9, which may be compared to experimental reference of LK73. As expected, the wave reaches its maximum amplitude just below the tropopause level, where a blocking zone develops. The $\theta$ and $U$ cross sections are in close agreement with observation throughout the troposphere. The mean vertical momentum flux resolved by the model has been computed as

$$M(Z) = \frac{1}{L}\int_L \rho(Z)U(X, Z)\cdot W(X, Z)dX$$

and is shown in Fig. 10a. The normalization length has been set at 200 km as in Lilly and Kennedy's paper. For comparison with previous studies, Fig. 13 of LK73, Fig. 19 of Klemp and Lilly (1978) and Fig. 9 of Hoinka (1985) have been reproduced here as Figs. 10b–d. The currently admitted mean value for the flux throughout the troposphere, in this case, is −0.6 Pa. Both previous model studies show that the flux is essentially constant throughout the troposphere, and rapidly decreasing in the turbulence layer (between 16 and 17 km in Klemp and Lilly's model, and between 13 and 16 km in Hoinka's model). This has been interpreted as the absorption of the wave by the nonlinearly generated critical layer near 17 km. This feature is well captured by our model. In addition, a small relative minimum of the flux is occurring near 11 km in Klemp and Lilly's model, near 7 km in Hoinka's model, and near 9.5 km in the observations. Our model is predicting larger vertical variations of the flux, with a maximum of −0.9 Pa near $Z = 4$ km and a minimum of −0.4 Pa near $Z = 8$ km. Part of these larger variations may be due to an insufficient horizontal resolution, since they decrease slightly when using $\Delta X = 2.5$ km (not shown). Given the general dispersion of previous results, however, we conclude that our model result falls within the range of possible values for this parameter.

The TKE cross section (Fig. 9d) shows that the model develops turbulence near the edge of the blocking zone, in agreement with the observations (Fig. 1 of LK73). This has been related by Klemp and Lilly to the observed rapid decrease of the wave-momentum flux at this level. In fact, the model confirms that this region is behaving as a nonlinearly generated critical level, which absorbs the upward-moving wave. It is particularly encouraging that the model is able to determine by its own dynamics the height and length scale of this turbulence zone. There is, unfortunately, no way of checking the quantitative value about the TKE observed in this case. Given the qualitative information on the spatial repartition of turbulence intensity contained in Fig. 1 of LK73, one may state that the model is producing a correct spatial pattern, but probably slightly underestimating the intensity of the TKE.

## 6. Simulation of the 11 January 1972 Chinook

Finally, we test the model on the famous Boulder windstorm (Lilly and Zipser 1972) for which numerous references of model studies exist. The upstream sounding is taken from Durran and Klemp (1983). To simulate this case, we retain $\Delta X = 5$ km, and use 40 levels with $\Delta Z = 500$ m. The absorbing layer is defined between 15 and 20 km. We use the same topography as in the former case. The model results after 6 h are shown in Fig. 11. They bear a strong resemblance with observations and previous model studies. The downslope wind velocity reaches nearly 60 m $\text{s}^{-1}$. Farther downstream, the flow appears to experience a hydraulic

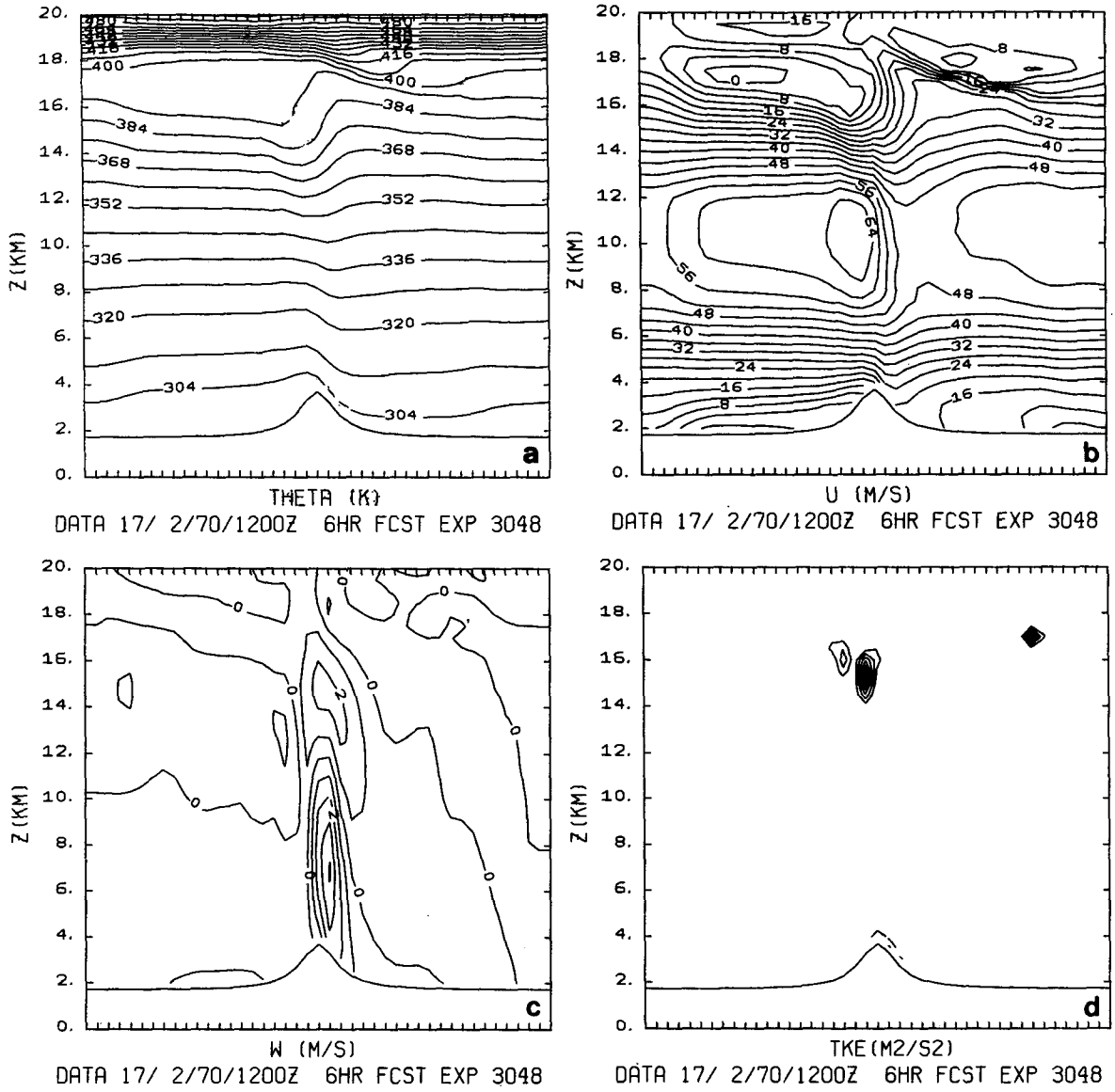


FIG. 9. Results of the simulation for 17 February 1970 after steady state is reached. (a) Potential temperature. (b) Horizontal wind. (c) Vertical velocity. (d) Turbulence kinetic energy [the isoline interval is $2(\text{m s}^{-1})^2$, starting at $2\,(\text{m s}^{-1})^2$]. For observational results, see LK73, Figs. 1 and 2. The mean flow is from the left to the right. Ticks are every 5 km on the horizontal axis.

jump. Many quantitative estimates given by Lilly (1978) allow for an assessment of the quality of the simulation. First, the wave momentum flux, computed as in the former case with $L = 200$ km, is shown in Fig. 12. It reaches a maximum value of $-8$ Pa near the mountain top and is generally decreasing with height in the troposphere, with an oscillation leading to a relative maximum near $Z = 7.5$ km. The observational estimates at 6 km (3.5 Pa) and 9 km (8 Pa) have been plotted on the figure. Although they provide only scarce evidence, they do not conflict with the oscillatory pattern. It is difficult to assess the confidence in these results. Klemp and Lilly (1978) preferred to use a mean value of 4.7 Pa in order to compare it with their model result. More confidence can be given to the fact that the wave momentum flux is generally decreasing throughout the troposphere, meaning that the wave energy is dissipated by the wave breaking mechanism. Next, the simulated surface wave drag has been computed as

$$D = -\frac{1}{L}\int_L p_s \frac{\partial h}{\partial X}\, dX,$$

with again $L = 200$ km, and compared to other model studies. Our model result gives $D = 9.4$ Pa, close to

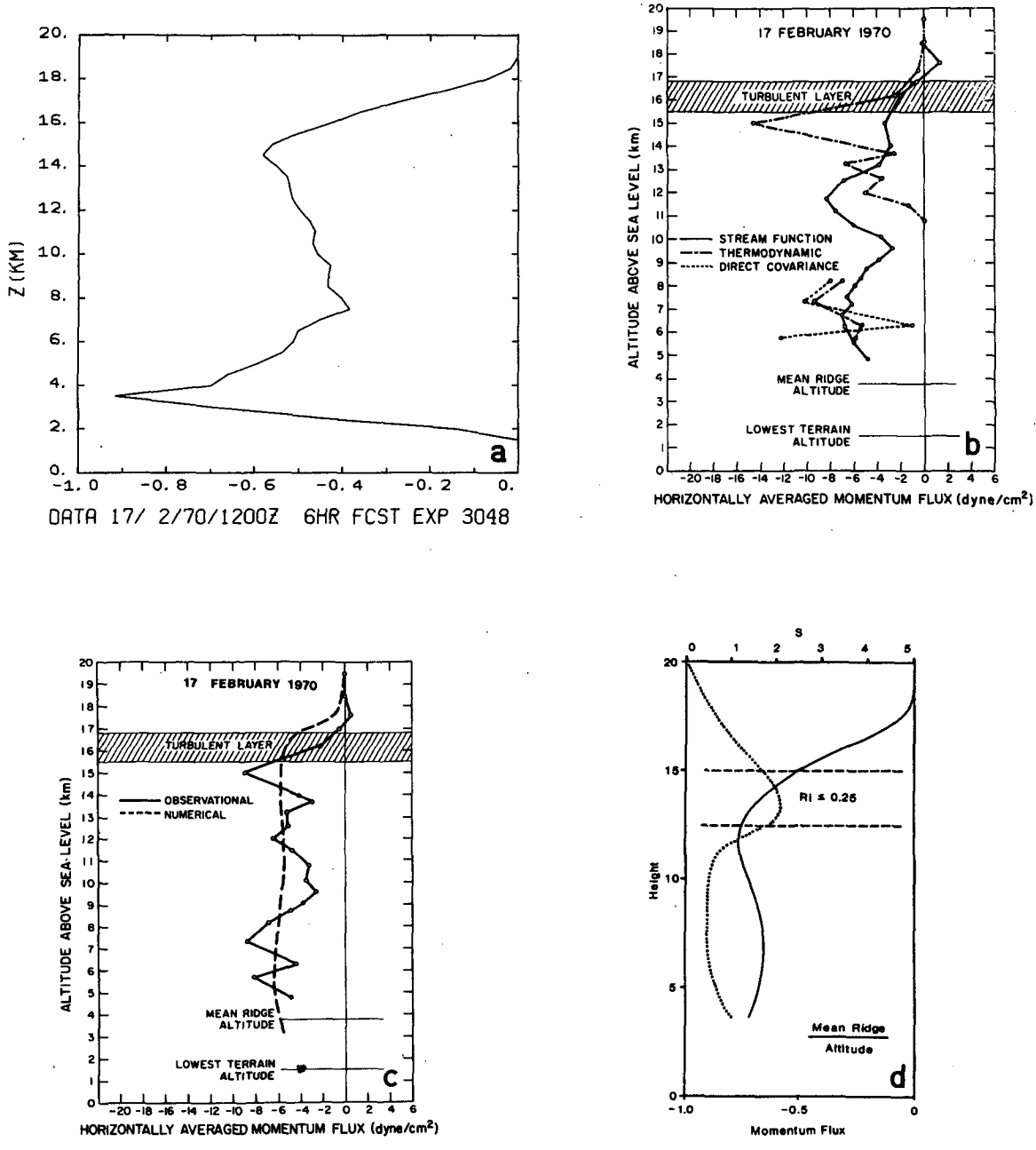


FIG. 10. The vertical wave momentum flux on 17 February 1970. (a) Present result; (b) observed, determined by different methods (Fig. 13 of LK73); (c) predicted by the numerical model of Klemp and Lilly (1978); (d) predicted by the model of Hoinka (1985) (solid line; the dashed line is the Richardson number). Units are Pa for (a) and (d), and 1 Pa = 10 dyn cm$^{-2}$.

the maximum values obtained by Hoinka (1985) (7 Pa), and Durran and Klemp (1983) or Peltier and Clark (1979) (8 Pa). Our model result is obtained after a 6 h forecast, and corresponds to a stationary state. On the other hand, in the three referenced numerical studies, the model had not reached steady state, as is obvious from the plots of surface drag versus time shown by the authors. Durran and Klemp, as well as Peltier and Clark, used nonhydrostatic models, with $\Delta X = 2$ km, and run their model about 2.5 hours with a free-slip lower boundary condition. Hoinka's model is hydrostatic with $\Delta X = 5$ km, and was run for until 10 hours again with a free-slip condition. We do not know why different models predict different time scales for the development of the Boulder windstorm. The major difference between our model and all three models mentioned previously, however, is that we do not use a free-slip boundary condition, but rather a

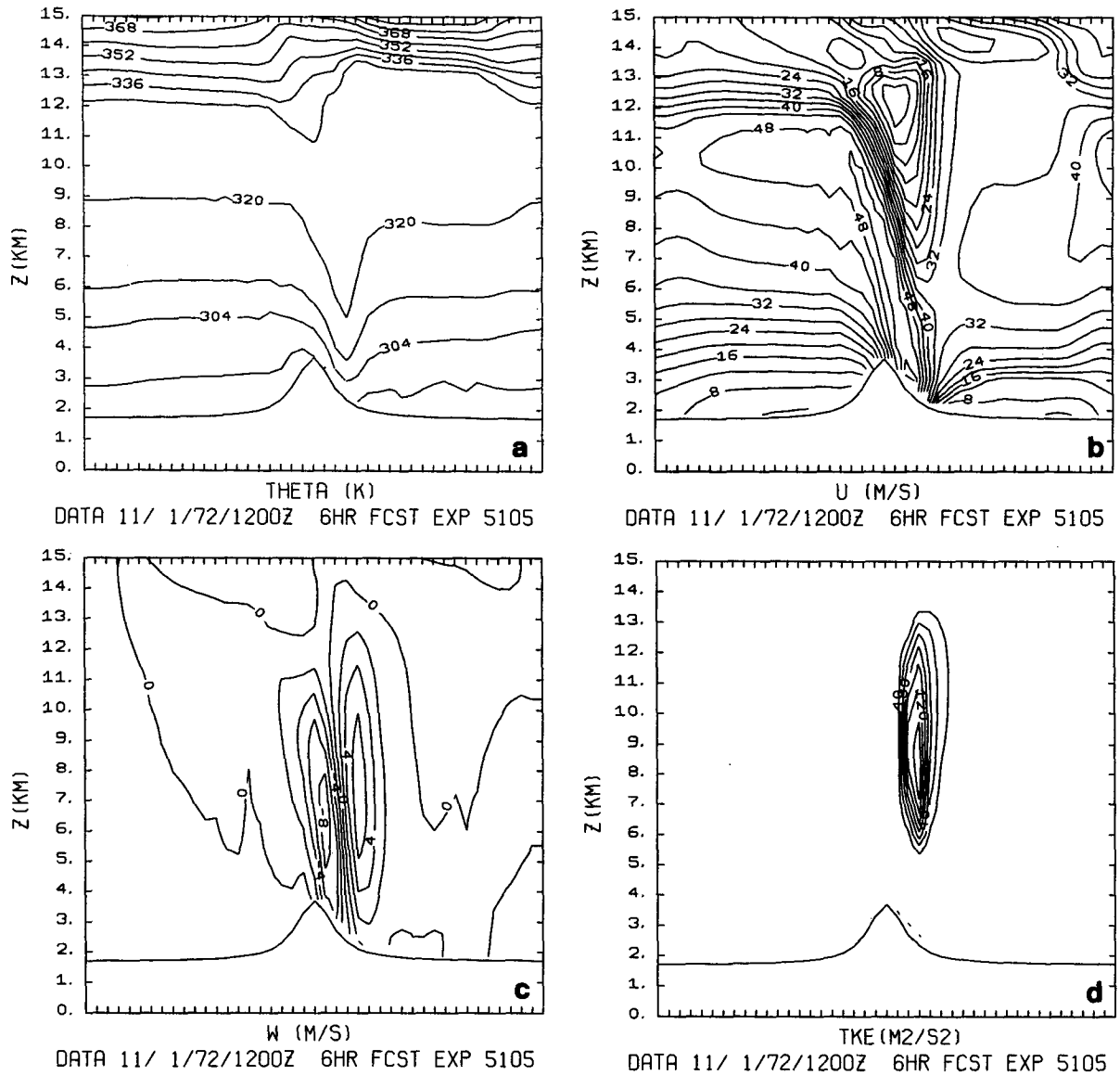


FIG. 11. Results of the simulation for 11 January 1972 after steady state is reached. (a) Potential temperature; (b) horizontal wind; (c) vertical velocity; (d) turbulence kinetic energy (the isoline interval is 20 $m^2 s^{-2}$, starting at 20 $m^2 s^{-2}$). For observational results, see, e.g., Klemp and Lilly (1978, Fig. 13a). The mean flow is from the left to the right of the picture. Ticks are every 5 km on the horizontal axis.

more realistic drag coefficient computed with a roughness height of 10 cm. This allows our model to reach a steady state after about 4 h of simulation, while other models clearly do not (this is illustrated in section 7). Here, we assume that the former authors have stopped their model simulations when the development of the windstorm had reached a realistic intensity, and therefore that the maximum values of the drag obtained during these simulations constitute a reasonable basis to appreciate the realism of our simulation. The mean surface turbulent drag over the same distance is estimated by our model as 0.62 Pa, whereas Lilly's estimate, based on a constant $C_D = 0.01$, is 1.5 hPa. Finally in our simulation, the surface pressure difference between two points at the altitude of 2600 m upstream and downstream of the mountain crest reaches the value of $-14.3$ hPa, a result very similar to Lilly's rough estimate of $-12$ hPa from direct pressure measurements. We may therefore conclude that the simulation of the mean flow by our model has a fair degree of realism.

We now discuss the TKE predicted by the model. Figure 11 shows that in the near-neutral, weak-wind zone that develops downstream of the crest, the TKE

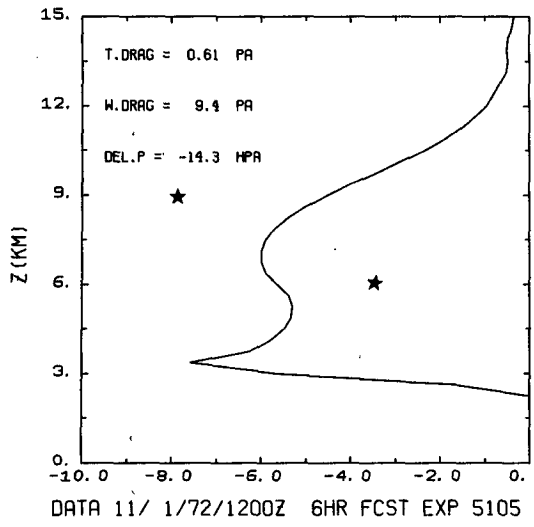


FIG. 12. The vertical wave momentum flux computed from the results shown in Fig. 11. Units are Pa, and symbols are observational results from Lilly (1978), as explained in the main text.

reaches very high values (about 140 $(\text{m s}^{-1})^2$ for the maximum). This is, again, in good agreement with Lilly's (1978) observations, since his estimate of the TKE intensity is 150 $(\text{m s}^{-1})^2$.

Moreover, the different terms in the TKE budget [Eq. (12)] are displayed on Fig. 13 and are in qualitative agreement with the observations. The leading term is the shear production, with an intensity reaching 1 $\text{m}^2\,\text{s}^{-3}$ (1.5 to 3 observed). The conversion into potential energy has a maximum value of $-0.2$ $\text{m}^2\,\text{s}^{-3}$ near 9 km and fits well with the observation. The model predicts the dissipation to lie within the range of $-0.2$ to $-0.4$ $\text{m}^2\,\text{s}^{-3}$ ($-0.8$ observed). Finally, the advection terms exhibit positive and negative values, with a maximum negative of $-0.4$ $\text{m}^2\,\text{s}^{-3}$ ($-0.6$ observed). Other terms (time change and vertical diffusion) were found to be of lesser importance. Although the agreement between the model and observed values for these different terms is not as good as for the TKE itself, we feel that the model has captured the gross features of the TKE budget. We may therefore conclude that the simulation of the turbulence induced by this extreme event is quite realistic.

Similar results have been recently obtained by Richard et al. (1988 personal communication), using a similar model based on a modified formulation of the Therry and Lacarrère (1983) turbulence scheme. The major difference with our study lies in a more empirical specification of the mixing and dissipative lengths. We feel that our formulation, based on Eq. (11), opens the possibility to the scheme being applied in more general cases, since, e.g., we have checked that PBL turbulence still scales properly.

## 7. Conclusions and perspectives

We have shown that the inclusion of the well-known turbulence kinetic energy equation in a mesobeta-scale model allows for successful predictions of the localization and intensity of clear-air turbulence in regions where the flow passes over steep orography. The success of the simulations is due to two aspects: 1) the good dynamical behavior of the model, which must have a sufficient vertical resolution to resolve the propagating internal wave, a sufficient horizontal resolution to resolve the main topographic features, and must not suffer from reflections at the top. This good dynamical behavior provides a good spatial distribution of the shear and of the static stability, which are the main parameters controlling the orography-induced turbulence. 2) The new formulation of the length scales, initially proposed by Bougeault and André (1986) for PBL studies, which turns out to be fairly general, since in most atmospheric flows, the length scale for turbulent eddies is primarily determined by the resistance to vertical displacements due to the static stability.

The accurate numerical simulation of the TKE opens several exciting possibilities. First, it allows for an improvement of the mean flow simulation, since it is well known that the waves are modified in regions of turbulent dissipation. To demonstrate this point, we have performed adiabatic frictionless simulations on the same three test cases. More precisely, the vertical diffusion terms in Eqs. (2) and (3) have been removed, but the horizontal diffusion terms were still present. The results after a 6 h simulation are shown in Fig. 14. For the bora and chinook cases, they are very different from those discussed in the previous sections. The shooting flow develops much further downstream and the flow seems to recover from the torrential regime only because of the downstream boundary condition. The momentum flux, computed as before, is much larger than in the dissipative runs. For the 17 February 1970 case, on the other hand, the change is not as obvious as for the two other cases, as there is no shooting flow. As is clearly visible in Fig. 14b, however, a statically unstable region develops at $Z = 18$ km, downstream of the crest. This leads to numerical instability after 9 h of simulation, whereas the dissipative runs were steady and absolutely stable. The comparison of the results with and without turbulence parameterization therefore shows a net improvement in the model behavior when the turbulence parameterization is included. This is not to say that previous schemes used to parameterize turbulent mixing are not good enough to simulate breaking mountain waves. In fact, with the former scheme used in this model, based on Louis et al. (1981) stability-dependent formulation of the eddy mixing coefficients, we obtained results of similar quality to those shown in this paper, as regard to the mean fields and the momentum fluxes. The major ad-

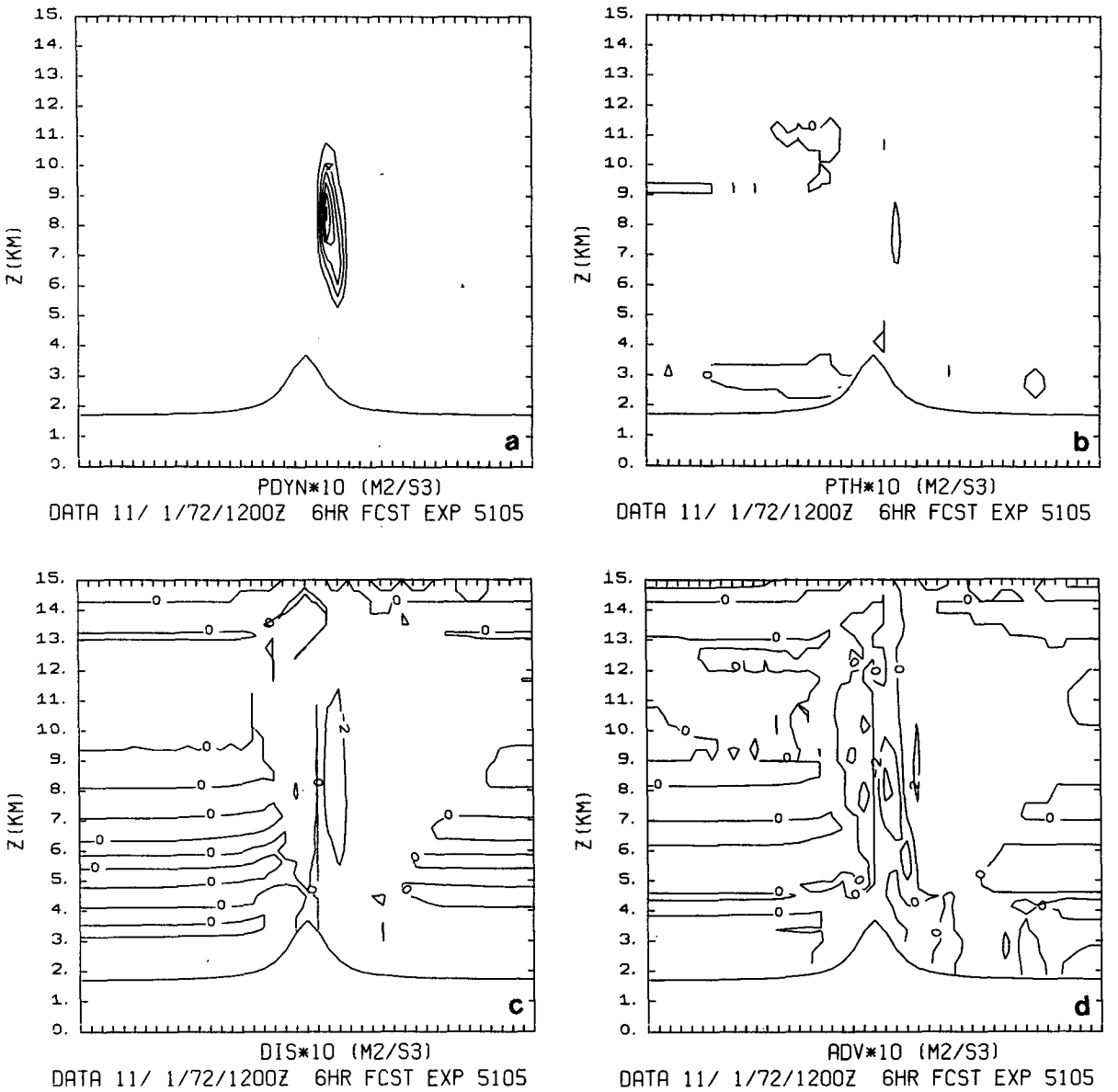


FIG. 13. The leading terms in the steady-state budget of TKE. (a) Shear production; (b) conversion into potential energy; (c) dissipation; (d) total advection. Units are $1/10\ m^2\ s^{-3}$. Interval between the isolines is $0.2\ m^2\ s^{-3}$.

vantage of this new approach is to provide a consistent prediction of the TKE intensity, allowing for experimental verification. Also, since it links the eddy diffusion coefficients to the TKE and to an interactively defined mixing length, one may hope that it will result in improvements in the simulation of the dynamic fields. This is, however, not yet demonstrated and would need more complete observational datasets.

Second, the present work may help to improve our theoretical understanding of orographic processes. We may already notice that the overall behavior of the flow in two of the three cases described here (bora and chinook) bears strong resemblance with the conceptual model of Smith (1985), which states that turbulence develops in a region of slowly moving air delimited by the two branches of a dividing streamline, while strong winds plunge underneath. The revival of the hydraulic theory, as opposed to the mechanism of linear resonant amplification proposed by Clark and Peltier (1984), has recently gained some support from numerical experiments by Durran and Klemp (1987). Until now, only higher resolution, nonhydrostatic models have provided a possibility to discriminate between these approaches, but at high computational cost. The present model may offer an interesting alternative; it also opens the possibility to improve the currently devel-

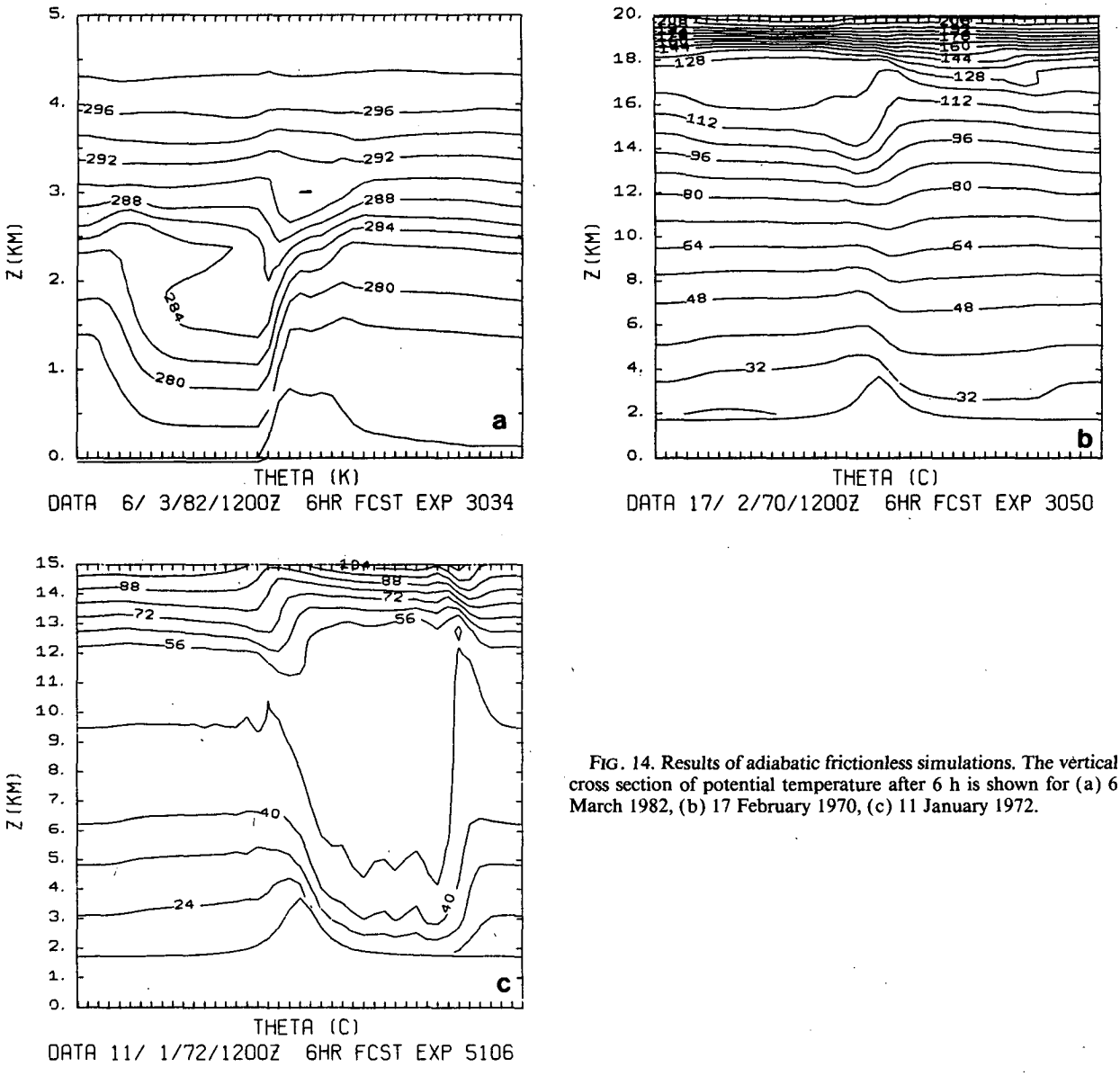


FIG. 14. Results of adiabatic frictionless simulations. The vertical cross section of potential temperature after 6 h is shown for (a) 6 March 1982, (b) 17 February 1970, (c) 11 January 1972.

oped parameterizations of the unresolved gravity wave drag effects in climate and NWP models. For instance, one may run the model in its 3D version over realistic topography to assess the degree of realism of the hypothesis that governs the vertical momentum deposit, or the low-level generation of momentum flux.

Finally, a number of studies in applied meteorology may take benefit from simulations of the TKE intensities; for instance, studies of atmospheric pollution dispersion, or of the best localization sites for astronomical sightings.

*Acknowledgments.* This study has greatly benefited from discussions with Drs. P. Pettré, E. Richard, and D. R. Durran. Computations were made at CCVR (Palaiseau) on resources allocated by the Direction de la Météorologie Nationale (Paris). The manuscript was prepared by D. Lacarrère.

## APPENDIX

## Summary of Numerical Methods

We provide here a short summary of the numerical methods used in the 3D version of the model. The 2D version is derived by setting to zero all the derivatives in the $y$ direction.

### 1. Vertical discretization

The model atmosphere is divided into $N$ layers of depth $\Delta\sigma$, separated by levels. By convention $\sigma = 0$ is the top of the atmosphere, $\sigma_N = 1$ is the surface and

$$\sigma_k = \exp\{-\Delta Z(N-k)g/R_aT_0\}. \quad \text{(A1)}$$

The layer $k$ extends from $\sigma_{k-1}$ to $\sigma_k$, with a depth $\Delta\sigma_k = \sigma_k - \sigma_{k-1}$, and a nominal $\sigma$ value

$$\sigma_{mk} = \frac{1}{2}(\sigma_k + \sigma_{k-1}). \quad \text{(A2)}$$

In the following $X_k$ will refer to the value of variable $X$ at level $\sigma_{mk}$, except for $\dot{\sigma}_k$ defined at level $\sigma_k$.

## 2. Hydrostatic equation

The value of the geopotential at any point in the model is obtained by integrating the hydrostatic equation upward, with the following discretization:

$$\phi_k = \phi_s + R_a \sum_{l=k+1}^{N} a_l T_l + b_k T_k, \quad \text{(A3)}$$

where

$$a_l = \mathrm{Ln}(\sigma_l/\sigma_{l-1}), \quad (l = 2, N),$$

$$b_l = a_l/2,$$

$$b_1 = \mathrm{Ln}2.$$

## 3. Conversion term

In Eq. (2), it is necessary to use a discretization of $\omega/p$ consistent with (A3) to obtain an accurate conversion of potential into kinetic energy. The discrete representation of $\sigma_{mk}^{-1}\int_0^{\sigma_{mk}} X d\sigma$ is noted $\hat{X}_k$ in the following, and defined as

$$\hat{X}_k = \frac{a_k}{\Delta\sigma_k}\sum_{l=1}^{k-1} X_l\Delta\sigma_l + b_k X_k, \quad \text{(A4)}$$

where $a_k$, $b_k$ are the previously defined coefficients. Thus the $\omega/p$ term in Eq. (2) is computed as

$$\left(\frac{\omega}{p}\right)_k = \frac{1}{p_s}\widehat{\nabla\cdot(p_s\mathbf{V})}_k + \sigma_{mk}\mathbf{V}_k\nabla Z. \quad \text{(A5)}$$

## 4. Mass continuity equation

Similarly, we will note

$$\tilde{X} = \sum_{l=1}^{N} X_l\Delta\sigma_l, \quad \text{(A6)}$$

and the mass continuity equation Eq. (1) restricted to the resolved dynamical terms, takes the form

$$\frac{\partial Z}{\partial t} = -\frac{1}{p_s}\widetilde{\nabla\cdot(p_s\mathbf{V})}. \quad \text{(A7)}$$

The generalized vertical velocity $\dot{\sigma}$ is then obtained from

$$\dot{\sigma}_0 = 0, \quad \dot{\sigma}_k - \dot{\sigma}_{k-1} = \frac{1}{p_s}\{\widetilde{\nabla\cdot(p_s\mathbf{V})} - \nabla\cdot(p_s\mathbf{V})_k\}. \quad \text{(A8)}$$

## 5. Horizontal discretization

An Arakawa $C$-type grid is used. We adopt the notations,

$$\overline{X}^x = \frac{1}{2}\left[X\left(x+\frac{\Delta x}{2}\right) + X\left(x-\frac{\Delta x}{2}\right)\right],$$

$$X_x = \frac{1}{\Delta x}\left[X\left(x+\frac{\Delta x}{2}\right) - X\left(x-\frac{\Delta x}{2}\right)\right], \quad \text{(A9)}$$

and further use the normalized value of the wind $U = u/m$, $V = v/m$, where $m$ is the map scale factor ($1/\Delta x$). Let

$$\eta = \frac{V_x - U_y + f}{\overline{p_s}^{xy}} \quad \text{(A10)}$$

be the potential vorticity, and

$$K = \frac{1}{2}(\overline{U^2}^x + \overline{V^2}^y) \quad \text{(A11)}$$

be the kinetic energy. Equations (1), (2), (3), restricted to the resolved dynamical part, take the form

$$\frac{\partial Z}{\partial t} = -\frac{m^2}{p_s}[(\overline{p_s}^x\tilde{U})_x + (\overline{p_s}^y\tilde{\mathbf{V}})_y], \quad \text{(A12)}$$

$$\frac{\partial T_k}{\partial t} = -\frac{m^2}{p_s}\frac{R_a}{C_p}T_k[(\overline{p_s}^x\hat{U}_k)_x + (\overline{p_s}^y\hat{V}_k)_y] + \frac{m^2}{p_s}\frac{R_a}{C_p}[\overline{\overline{p_s}^x U_k\overline{T_k}^x Z_x}^x + \overline{\overline{p_s}^y V_k\overline{T_k}^y Z_y}^y] - \frac{m^2}{p_s}[\overline{\overline{p_s}^x U_k T_{kx}}^x + \overline{\overline{p_s}^y V_k T_{ky}}^y], \quad \text{(A13)}$$

$$\frac{\partial U_k}{\partial t} = -[\phi_x + R_a\overline{T_k}^x Z_x] + \overline{\eta}^y\overline{\overline{p_s}^y V}^{xy} - K_x, \quad \text{(A14)}$$

$$\frac{\partial V_k}{\partial t} = -[\phi_y + R_a\overline{T_k}^y Z_y] - \overline{\eta}^x\overline{\overline{p_s}^x U}^{xy} - K_y. \quad \text{(A15)}$$

## 6. Time discretization

The model is integrated with a leapfrog time scheme, the decoupling between even and odd time steps being prevented by the use of a time filter. For the average $\Delta x = 5$ km used here, the time step is $\Delta t = 30$ s. This is made possible by a semi-implicit treatment for the linear part of the gravity-wave solutions of (A12)–(A15), and a further implicit treatment of the vertical diffusion terms. The detail of these computations is not given here.

## 7. Lateral Boundary Forcing

The boundary relaxation terms in Eqs. (1), (2), (3) are also treated in an implicit way. The result takes the simple following form: let $X^c$ be the value of variable $X$ computed without the relaxation term, and

$X_{1-s}$ the assumed large-scale value of this variable, the final value of $X$ is given by

$$(1 - \alpha)X^c + \alpha X^{1-s},$$

$\alpha$ taking the values, 1.0, 0.45339, 0.20556, 0.09320, 0.04226, 0.01916, and 0.0 for grid points distant from the lateral boundary by, respectively, 0, 1, 2, 3, 4, 5, and more grid points.

## REFERENCES


Alpert, P., and J. Neumann, 1984: On the enhanced smoothing over topography in some meteorological models. *Bound.-Layer. Meteor.*, **30,** 293–312.

André, J. C., and P. Lacarrère, 1980: Simulation numérique détaillée de la couche limite atmosphérique. Comparaison avec la situation des 2 et 3 Juillet 1977 à Voves. *La Météorologie,* **VI(22),** 5–49.

Beljaars, A. C. M., J. L. Walmsley and P. A. Taylor, 1987: A mixed spectral finite-difference model for neutrally stratified boundary layer flow over roughness changes and topography. *Bound.-Layer Meteor.*, **38,** 273–303.

Bougeault, Ph., 1986: The Peridot model: A qualification study at the meso-beta-scale. EERM internal note *n°* 168.*

——, 1987: Study of some orographic flows with the Peridot model. First part: Qualification of the model. EERM internal note n° 191.*

——, 1988: Simulations of orographic flows with a 10 km-scale hydrostatic model. *Proc. ECMWF Workshop on Techniques for Horizontal Discretization in NWP Models,* [Available from ECMWF, Shinfield Park, Reading, RG29AX Berkshire, UK.]

——, and J. C. André, 1986: On the stability of the third-order turbulence closure for the modeling of the stratocumulus-topped boundary layer. *J. Atmos. Sci.*, **43,** 1574–1581.

Buty, D., 1988: Parameterization of atmospheric turbulence in three-dimensional, non-hydrostatic, meso meteorological model. Ph.D. thesis, Ecole Central du Lyon 145 pp. [Available from EDF Etudes et Recherches, 6 Quai Watier, 78400 CHATOU, France.]

Clark, T. L., and W. R. Peltier, 1984: Critical level reflection and the resonant growth of nonlinear mountain waves. *J. Atmos. Sci.*, **41,** 3122–3134.

Deardorff, J. W., 1972: Theoretical expressions for the counter gradient vertical heat flux. *J. Geophys. Res.*, **30,** 5900–5904.

——, 1974: Three-dimensional numerical study of turbulence in an entraining mixed layer. *Bound.-Layer Meteor.*, **7,** 199–226.

Durran, D. R., 1986: Another look at downslope windstorm. Part I: The development of analogs to super critical flow in an infinitely deep, continously stratified fluid. *J. Atmos. Sci.*, **43,** 2527–2543.

——, and J. B. Klemp, 1983: A compressible model for the simulation of moist mountain waves. *Mon. Wea. Rev.*, **111,** 2341–2361.

——, and ——, 1987: Another look at downslope winds. Part II: Nonlinear amplification beneath wave-overturning layers. *J. Atmos. Sci.*, **44,** 3402–3412.

Fua, D., G. Chimona, F. Einaudi and O. Zeman, 1982: An analysis of wave-turbulence interactions. *J. Atmos. Sci.*, **39,** 2450–2463.

Hoinka, D. R., 1985: A comparison of numerical simulation of hydrostatic flow over mountain with observations. *Mon. Wea. Rev.*, **113,** 719–735.

Imbard, M., A. Joly and R. Juvanon du Vachat, 1986: The Peridot model for NWP: Formulation and Manual. EERM internal note n° 161.*

Klemp, J. B., and D. K. Lilly, 1978: Numerical simulation of hydrostatic mountain waves. *J. Atmos. Sci.*, **35,** 78–107.

——, and D. R. Durran, 1987: Numerical modelling of Bora winds. *Meteor. Atmos. Phys.*, **36,** 215–227.

Lenschow, D. H., J. C. Wyngaard and W. T. Pennel, 1980: Mean field and second-moment budgets in a baroclinic, convective, boundary-layer. *J. Atmos. Sci.*, **37,** 1313–1326.

Lilly, D. K., 1962: On the numerical simulation of buoyant convection. Tellus, **4,** 145–172.

——, 1978: A severe downslope windstorm and aircraft turbulence event induced by mountain wave. *J. Atmos. Sci.*, **35,** 59–77.

——, and E. J. Zipser, 1972: The front range windstorm of 11 January 1972. A meteorological narrative. *Weatherwise,* **25,** 56–63.

——, and P. J. Kennedy, 1973: Observations of a stationary mountain wave and its associated momentum flux and energy dissipation. *J. Atmos. Sci.*, **30,** 1135–1152.

——, D. E. Waco and S. I. Adelfang, 1974: Stratospheric mixing estimated from high altitude turbulence measurements. *J. Appl. Meteor.*, **13,** 488–493.

Louis, J. F., M. Tiedtke and J. F. Geleyn, 1981: A short history of the operational PBL-parameterization of ECMWF. *Workshop on Planetary Boundary Layer Parameterization,* ECMWF, 59–79.

Orlanski, I., 1975: A rationale subdivision of scales for atmospheric processes. *Bull. Amer. Meteor. Soc.*, **56,** 527–530.

Peltier, W. R., and T. L. Clark, 1979: The evolution and stability of finite amplitude mountain waves. Part II: Surface wave drag and severe downslope windstorms. *J. Atmos. Sci.*, **36,** 1498–1529.

Pettré, P., 1988: Descriptive experimental analysis of two Bora cases using ALPEX aircraft data. *Contrib. Atmos. Phys.*, **61,** 143–150.

Pielke, R. A., 1984: *Mesoscale Meteorological Modeling.* Academic Press, 612 pp.

Richard, E., J. P. Pinty and N. Chaumerliac, 1985: Simulation of hydrostatic bidimensional mountain waves. Note IOPG n° 82, 50 pp. [Available from LAMP, BP 45 63170 Aubière, France.]

Smith, R. B., 1985: On severe downslope winds. *J. Atmos. Sci.*, **42,** 2597–2603.

——, 1987: Aerial observations of the Yugoslavian Bora. *J. Atmos. Sci.*, **44,** 269–297.

Therry, G., and P. Lacarrère, 1983: Improving the eddy kinetic energy model for planetary boundary layer description. *Bound.-Layer Meteor.*, **25,** 63–88.

Weinstock, J., 1978: Vertical turbulent diffusion in a stably stratified fluid. *J. Atmos. Sci.*, **35,** 1022–1027.

——, 1987: The turbulence field generated by a linear gravity wave. *J. Atmos. Sci.*, **44,** 410–420.

Willis, G. E., and J. W. Deardorff, 1974: A laboratory model of the unstable Planetary Boundary Layer. *J. Atmos. Sci.*, **31,** 1297–1307.


* All EERM Internal Notes are available from CNRM, 42, av. Coriolis, 31057TOULOUSE Cedex France.